Click-to-lead design of a picomolar ABA receptor antagonist with potent activity in vivo

Aditya S. Vaidya[a,b], Francis C. Peterson[c], James Eckhardt[a,b], Zenan Xing[a,b], Sang-Youl Park[a,b], Wim Dejonghe[a,b], Jun Takeuchi[d,e], Oded Pri-Tal[f], Julianna Faria[a,b], Dezi Elzinga[a,b], Brian F. Volkman[c], Yasushi Todoroki[d,e], Assaf Mosquna[f], Masanori Okamoto[g], and Sean R. Cutler[a,b,1]

[a]Institute for Integrative Genome Biology, University of California, Riverside, CA 92521; [b]Botany and Plant Sciences, University of California, Riverside, CA 92521; [c]Department of Biochemistry, Medical College of Wisconsin, Milwaukee, WI 53226; [d]Faculty of Agriculture, Shizuoka University, Shizuoka 422-8529, Japan; [e]Research Institute of Green Science and Technology, Shizuoka University, Shizuoka 422-8529, Japan; [f]The Robert H. Smith Institute of Plant Sciences and Genetics in Agriculture, The Hebrew University of Jerusalem, Rehovot 7610001, Israel; and [g]Center for Bioscience Research and Education, Utsunomiya University, Utsunomiya 321-8505, Japan

This contribution is part of the special series of Inaugural Articles by members of the National Academy of Sciences elected in 2018.

Contributed by Sean R. Cutler, May 3, 2021 (sent for review May 3, 2021; reviewed by Michael Hothorn and Yoshikatsu Matsubayashi)

Abscisic acid (ABA) is a key plant hormone that mediates both plant biotic and abiotic stress responses and many other developmental processes. ABA receptor antagonists are useful for dissecting and manipulating ABA's physiological roles in vivo. We set out to design antagonists that block receptor–PP2C interactions by modifying the agonist opabactin (OP), a synthetically accessible, high-affinity scaffold. Click chemistry was used to create an ∼4,000-member library of C4-diversified opabactin derivatives that were screened for receptor antagonism in vitro. This revealed a peptidotriazole motif shared among hits, which we optimized to yield antabactin (ANT), a pan-receptor antagonist. An X-ray crystal structure of an ANT–PYL10 complex (1.86 Å) reveals that ANT's peptidotriazole headgroup is positioned to sterically block receptor–PP2C interactions in the 4′ tunnel and stabilizes a noncanonical closed-gate receptor conformer that partially opens to accommodate ANT binding. To facilitate binding-affinity studies using fluorescence polarization, we synthesized TAMRA–ANT. Equilibrium dissociation constants for TAMRA–ANT binding to *Arabidopsis* receptors range from ∼400 to 1,700 pM. ANT displays improved activity in vivo and disrupts ABA-mediated processes in multiple species. ANT is able to accelerate seed germination in *Arabidopsis*, tomato, and barley, suggesting that it could be useful as a germination stimulant in species where endogenous ABA signaling limits seed germination. Thus, click-based diversification of a synthetic agonist scaffold allowed us to rapidly develop a high-affinity probe of ABA–receptor function for dissecting and manipulating ABA signaling.

antagonist | abscisic acid | receptor | click chemistry | ligand

The phytohormone abscisic acid (ABA) controls numerous physiological processes in plants ranging from seed development, germination, and dormancy to responses for countering biotic and abiotic stresses (1). ABA binds to the PYR/PYL/RCAR (*Pyrabactin Resistance 1/PYR1-like/Regulatory Component of ABA Receptor*) soluble receptor proteins (2, 3) and triggers a conformational change in a flexible "gate" loop flanking the ligand-binding pocket such that the ABA–receptor complex can then bind to and inhibit clade A type II C protein phosphatases (PP2Cs), which normally dephosphorylate and inactivate SNF1-related protein kinase 2 (SnRK2). This, in turn, leads to SnRK2 activation, phosphorylation of downstream targets, and multiple cellular outputs (4, 5).

Chemical modulators of ABA perception have been sought as both research tools for dissecting ABA's role in plant physiology and for their potential agricultural utility (6, 7). Dozens of ABA receptor agonists, which reduce transpiration and water use by inducing guard cell closure, have been developed and are being explored as chemical tools for mitigating the effects of drought on crop yields (7–23), most of them either being analogs of ABA or sulfonamides similar to quinabactin (24). ABA receptor antagonists could conceivably be useful in cases where water is not limiting, for example, to increase transpiration and gas exchange under elevated CO_2 in glasshouse agriculture, as germination stimulators, and for studying the ABA dependence of physiological processes, among other applications (25–31). Thus, both ABA receptor agonists and antagonists have potential uses as research tools and for plant biotechnology.

In principle, there are at least two mechanisms for blocking ABA receptor activation: by preventing gate closure, which is necessary for PP2C binding, or by sterically disrupting the activated, closed-gate receptor conformer from binding to PP2Cs. Prior efforts to design antagonists have focused on the latter strategy and include multiple ABA-derived ligands such as AS6 (25), PanMe (26), 3′-alkyl ABA (30–32), 3′-(phenyl alkynyl) ABA (33), or ligands derived from tetralone ABA (34) with varying degrees of conformational restriction (27, 28, 35). With the exception of PanMe, these antagonists have linkers attached to the 3′ carbon of ABA or 11′ carbon of tetralone ABA, which is positioned to disrupt receptor–PP2C interactions by

Significance

Abscisic acid (ABA) is a phytohormone that plants utilize to coordinate responses to abiotic stress, modulate seed dormancy, and is central to plant development in several contexts. Chemicals that activate or block ABA signaling are useful as research tools and as potential agrochemical leads. Many successes have been reported for ABA activators (agonists), but existing ABA blockers (antagonists) are limited by modest in vivo activity. Here we report antabactin (ANT), a potent ABA blocker developed using "click chemistry"–based diversification of a known ABA activator. Structural studies reveal, ANT disrupts signaling by stabilizing ABA receptors in an unproductive form. ANT can accelerate seed germination in multiple species, making it a chemical tool for improving germination.

Author contributions: A.S.V., F.C.P., J.E., Z.X., S.-Y.P., J.T., O.P.-T., B.F.V., Y.T., A.M., M.O., and S.R.C. designed research; A.S.V., F.C.P., J.E., Z.X., S.-Y.P., J.T., O.P.-T., J.F., D.E., Y.T., A.M., and M.O. performed research; A.S.V. and W.D. contributed new reagents/analytic tools; A.S.V., F.C.P., J.E., Z.X., J.T., O.P.-T., Y.T., A.M., and M.O. analyzed data; A.S.V. and S.R.C. wrote the paper; and D.E. conducted exploratory receptor–probe binding studies.

Reviewers: M.H., Universite de Geneve; and Y.M., Nagoya Daigaku.

Competing interest statement: A.S.V. and S.R.C. are co-inventors on a University of California, Riverside–owned patent application relating to materials described in this manuscript.

See online for related content such as Commentaries.

[1]To whom correspondence may be addressed. Email: sean.cutler@ucr.edu.

This article contains supporting information online at https://www.pnas.org/lookup/suppl/doi:10.1073/pnas.2108281118/-/DCSupplemental.

Published September 16, 2021.

protruding through the 3′ tunnel. PanMe was created by modifying ABA's C4′ (Fig. 1) with a toluylpropynyl ether substituent designed to occupy the 4′ tunnel, a site of close receptor–PP2C contact (26). Structural studies showed that this 4′ moiety adopts two conformations, one that resides in the 4′ tunnel and another that occupies the adjacent 3′ tunnel (26). Collectively, these elegant studies have demonstrated that antagonists of receptor–PP2C interactions can be designed by modifying agonists at sites situated proximal to the 3′ or 4′ tunnels. Despite these advances, current antagonists have limitations. For example, PanMe, which has low nanomolar affinity for the subfamily II receptor PYL5, is limited by relatively low activity on subfamily I and III ABA receptors, and as we show here, the ABA antagonist AA1 (36) (Fig. 1) lacks detectable antagonist activity in vitro and is, therefore, unlikely to be a true ABA receptor antagonist. Together, these data suggest that higher-affinity pan-antagonists and/or molecules with increased bioavailability will be necessary to more efficiently block endogenous ABA signaling. We set out to address these limitations by modifying the scaffold of the synthetic ABA agonist opabactin (OP), which has an approximately sevenfold increase in both affinity and bioactivity relative to ABA (21). We describe an OP derivative called antabactin (ANT) and show that it is a high-affinity binder and antagonist of ABA receptors that disrupts ABA-mediated signaling in vivo.

Results and Discussion

Discovery of ABA Receptor Antagonists by Click Chemistry Mediated Scaffold Elaboration. OP possesses a C4-nitrile substituent that is superimposable with ABA's C4′-ring ketone in ternary receptor/ligand/complexes (21). We hypothesized that this position could be used to design high-affinity antagonists by appending moieties that block receptor–PP2C interactions (Fig. 2*A*), analogously to C4′-modified ABA-based antagonists like PanMe (Fig. 1). To create a library of C4-modified OP analogs, we designed OPZ, which replaces OP's 4-nitrile substituent with an azide that can be diversified into OP-4-triazoles using Cu(I) catalyzed 1–3 dipolar alkyne-azide cycloadditions (click chemistry; Fig. 2*B* and *SI Appendix*, Fig. S1*A*). ABA receptor activity is conveniently measured in vitro by ligand- and receptor-dependent inhibition of clade A PP2C phosphatase activity; antagonism of this can be measured by the antagonist-mediated recovery of PP2C activity in the presence of saturating ABA. Characterization of OPZ by PP2C recovery assays showed that it is a weak partial antagonist of ABA-mediated PP2C inhibition, indicating that it retains receptor binding activity (*SI Appendix*, Fig. S2). We additionally observed that unpurified click reactions, BTTAA ligand, Cu++, and ascorbate can all be added to PP2C recovery assays with minimal effect on phosphatase activity, which enables direct and rapid screening of unpurified click reactions (*SI Appendix*, Fig. S2). With this assay for rapid synthesis and screening established, we assembled a library of ∼4,000 alkynes from commercial vendors and used these to synthesize a collection of OP-4-triazoles in microtiter plates. The crude reactions were assayed directly for antagonism of PYR1 activity without purification; 204 of the reactions contained products that enabled recovery of >90% of PP2C activity when present at a 10-fold theoretical excess over saturating ABA (5,000 nM). The hits clustered into 10 scaffolds, although most were derived from reactions with propargyl amides that create OP-4-peptidotriazoles (*SI Appendix*, Fig. S3 and Dataset S1). The alkyne library that we screened contained 735 propargyl amides (out of 4,002 compounds in total). Of the total of 204 hits, 121 (∼59%) were propargyl amides, which indicates significant enrichment among hits (P < 2e-38, χ^2 test). To optimize activity, we synthesized a focused library of aryl/heteroaryl propargyl amides using polymer-supported chemistry to link propargyl amine to carboxylates similar to our best hits. The resultant propargyl amides were clicked against OPZ and assayed for antagonist activity (Dataset S2). These efforts ultimately yielded a quinoline peptidotriazole with an improved activity that we have named antabactin (antagonist of ABA action or ANT) (Fig. 2*B* and *SI Appendix*, Fig. S1*B*). In vitro pulldown assays demonstrate that ANT disrupts ABA-mediated receptor–PP2C interactions, as expected, based on our structure-guided design strategy (*SI Appendix*, Fig. S4).

To compare ANT's activity to PanMe and AA1, we used PP2C recovery assays in the presence of ABA using a panel of 10 *Arabidopsis* and eight wheat receptors that span the three clades of angiosperm ABA receptors. These data show ANT is a highly active pan-receptor antagonist that disrupts ABA-mediated receptor activation at concentrations up to 50-fold lower than ABA (Fig. 2*C* and *SI Appendix*, Fig. S5). In comparison to other antagonists, ANT is between 5.6- and 430-fold more potent than PanMe and has high activity across all receptors tested (Fig. 2*C* and *SI Appendix*, Fig. S5). Unexpectedly, we observed that AA1 does not antagonize *Arabidopsis*, wheat, or Brachypodium ABA receptors in vitro (Fig. 2*C* and *SI Appendix*, Figs. S5 and S6), in contrast to previous reports (32). ANT's improved activity in vitro is paralleled in vivo, which we measured by quantifying reversal of ABA-mediated inhibition of seedling establishment (Fig. 2*D* and *SI Appendix*, Fig. S7*A*). In these assays, ANT is ∼2.5- and 34-fold more potent than PanMe and AA1, respectively (Fig. 2*D*). In addition, we note that PanMe has a complex dose–response curve that suggests possible phytotoxicity unrelated to ABA, since PanMe's high-concentration growth inhibition was also observed in the *abi1-1* mutant strain (Fig. 2*D* and *SI Appendix*, Fig. S7 *B* and *C*). Collectively, our data demonstrate that ANT is a highly active pan-receptor ABA antagonist that disrupts signaling by preventing receptor–PP2C interactions.

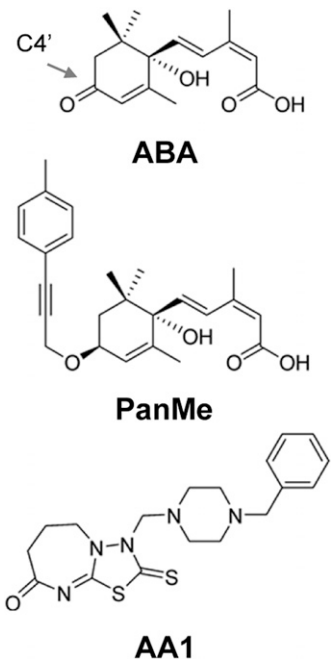

Fig. 1. Structures of ABA, PanMe, and AA1.

ANT Is Positioned to Block PP2C Binding. To better understand the molecular basis of ANT's mechanism of action, we solved the structure of a PYL10$^{25\text{-}183}$–ANT binary complex using X-ray crystallography to a resolution of 1.80 Å. The complex crystallized in the C121 space group and contained a single protomer in the asymmetric unit. Several iterations of structural refinement were conducted prior to modeling ANT into the PYL10 ligand-binding pocket's unbiased electron density (*SI Appendix*, Fig. S8 *A–C*). A real-space correlation coefficient of 0.97 calculated between the unbiased electron density and ANT indicates good agreement between our model and the observed electron density.

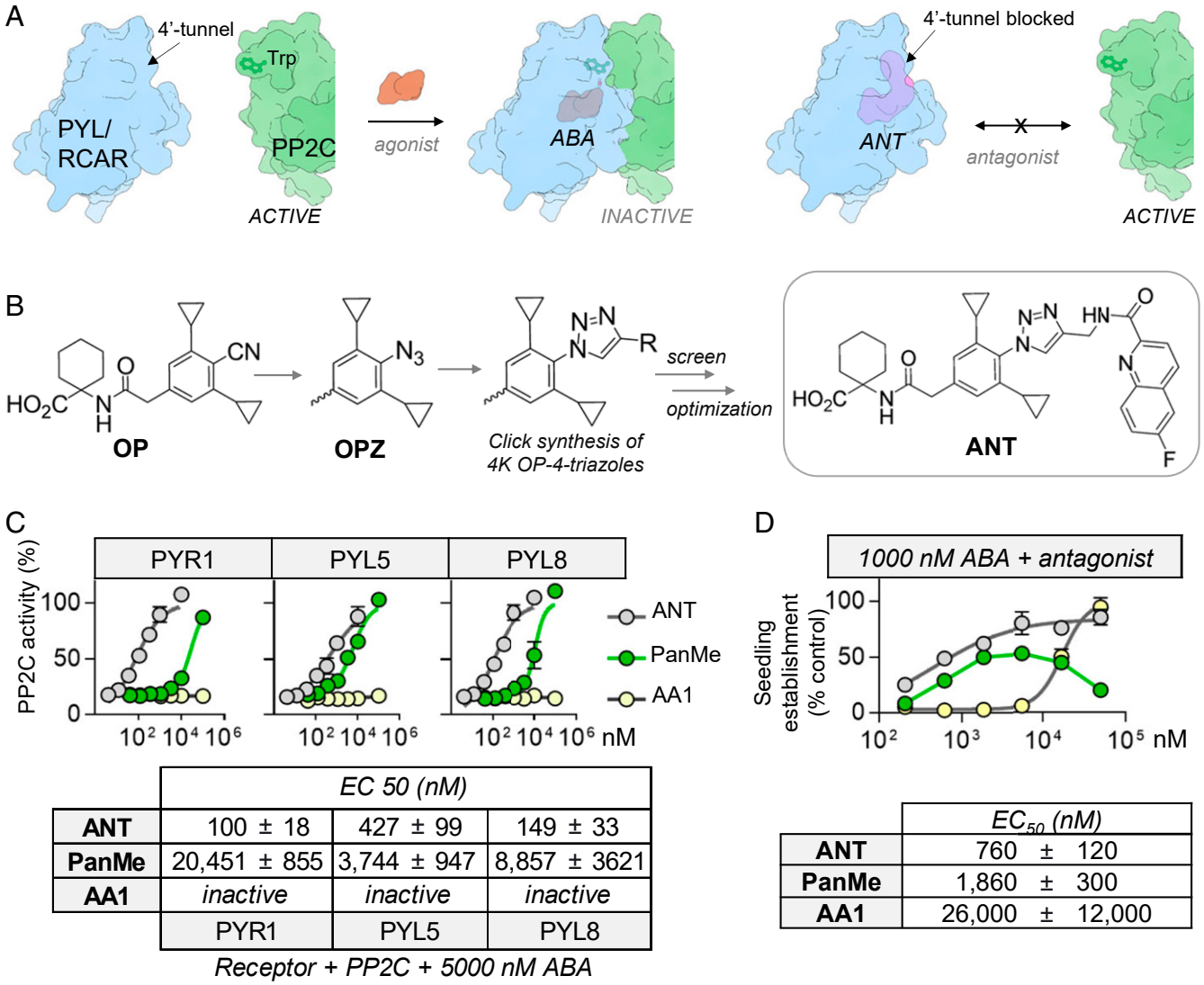

	EC 50 (nM)		
ANT	100 ± 18	427 ± 99	149 ± 33
PanMe	20,451 ± 855	3,744 ± 947	8,857 ± 3621
AA1	*inactive*	*inactive*	*inactive*
	PYR1	PYL5	PYL8

Receptor + PP2C + 5000 nM ABA

	EC_{50} (nM)
ANT	760 ± 120
PanMe	1,860 ± 300
AA1	26,000 ± 12,000

Fig. 2. Rapid discovery of 4-OP-triazole ABA receptor antagonists. (*A*) Comparison of agonist and antagonist mechanisms. ABA stabilizes a PYL/RCAR–PP2C complex and inactivates PP2C activity. Antagonists that disrupt PP2C interactions block agonist-mediated PP2C inactivation. (*B*) Discovery of ANT using click chemistry ligand diversification. The ABA receptor agonist OP was diversified at its C4 nitrile position to identify substituents that disrupt PP2C interactions in the 4′ tunnel. OPZ is a C4-azido derivative of OP; OPZ was clicked against a collection of alkynes and the reactions were screened in vitro to identify antagonists. Subsequent optimization led to ANT. (*C*) ANT is a potent ABA receptor antagonist. The potency of ANT, PanMe, and AA1 receptor antagonism was quantified by measuring the antagonist-mediated recovery of PP2C activity in the presence of saturating ABA (5,000 nM), PYL/RCAR, and ΔN-HAB1 proteins (both at 25 nM). EC_{50} values were obtained by nonlinear fits of dose–response data to the four parameter log-logistic equation using the drc R package (47); assays were conducted in triplicate. The full dataset for all *Arabidopsis* and wheat receptors is presented in *SI Appendix*, Fig. S4. (*D*) ANT is active in vivo. Antagonist-dependent recovery of seedling establishment in the presence of ANT, PanME, or AA1 (+1,000 nM ABA). Seedling growth was measured by quantifying the green cotyledon area normalized to seed number 4 d after stratification; EC_{50} values indicate the concentration of the antagonist at 50% maximal green pixel area relative to mock control (1,000 nM ABA); errors indicate SD of two independent experiments each conducted in triplicate.

A second crystal structure was also obtained at a resolution of 1.77 Å for a quinoxaline analog 4a of ANT, and this displayed a consistent ligand placement (*SI Appendix*, Fig. S8 *D–F*).

The structure of the ANT–PYL10 complex is broadly consistent with the initial design strategy—that of OP modified to disrupt receptor–PP2C interactions at the 4′ tunnel. The structure reveals that ANT–PYL10 interactions are stabilized by a combination of water-mediated and direct H bonds, numerous hydrophobic contacts, and π–π/π–cation interactions (Fig. 3*A* and *SI Appendix*, Fig. S8). ANT's carboxylate forms a salt bridge to K56, makes extensive water-mediated contacts with polar residues lining PYL10's ligand-binding pocket and hydrophobic interactions with the C6 tunnel (which normally accommodates ABA's C6 methyl and modulates ABA binding affinity) (23) (*SI Appendix*, Fig. S8*G*). In addition, the structure illuminates the importance of ANT's peptidotriazole head group to binding, which is stabilized by a network of polar contacts between the gate and latch loops and the peptidotriazole module and π–π/π–cation interactions. These position ANT's quinoline ring in the 4′ tunnel and occlude access to the solvent-exposed pocket that would normally contact the PP2C's Trp lock in an activated receptor–ligand–PP2C complex (Fig. 3*C*). ANT's triazole forms direct contacts to amide NH of A85 of the gate loop, and ANT's peptide bond forms contacts with the amide NHs of R112 and L113 in the "latch" loop. ANT's quinoline ring system forms a π–cation interaction with the latch R112 guanidinium, engages in π–π stacking interactions with F155 phenyl side chain, and forms an H bond between R112's guanidinium and the quinoline's nitrogen (Fig. 3*A*).

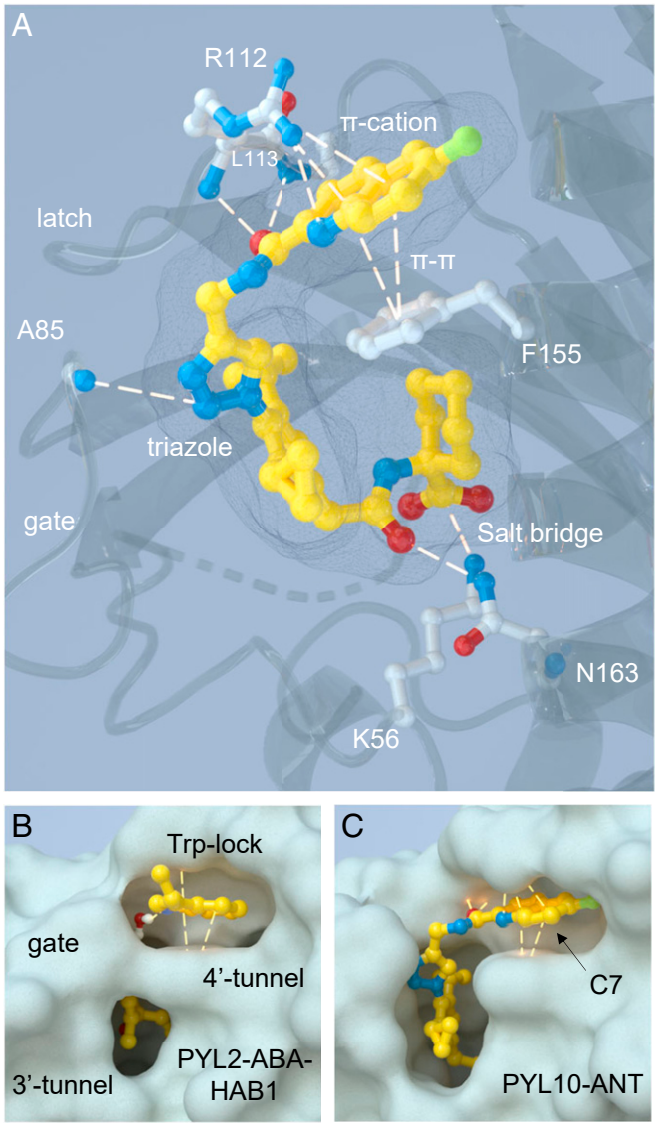

Fig. 3. ANT–receptor binding is stabilized by numerous direct contacts and occludes the 4′ tunnel. (*A*) The cocrystal structure of ANT bound to PYL10, highlighting direct receptor–ligand contacts, as determined using PLIP analyses (48). The dashes represent polar contacts established by ANT with PYL10 and include direct hydrogen bonds, which range in distance from 2.7 to 3.8 Å (see *SI Appendix*, Fig. S8*G* for all distances), π–π parallel stacking (distances 4.1 and 4.2 Å angle 14.07° and 14.19° and offset 1.73 and 1.64 Å), and π–cation interactions (distances 3.9 and 4.3 Å and offset 0.57 and 1.95 Å) interactions and salt bridge (2.8 Å). (*B*) Trp-lock insertion from HAB1 into the 4′ tunnel formed in an activated PYL2–ABA analog–HAB1 ternary complex (PDB, accession no. 5OR2). (*C*) ANT's quinoline ring occupies the 4′ tunnel that would normally be occupied by the Trp-lock residue, sterically blocking access of Trp from HAB1. Noted is the solvent-exposed C7 position on the quinoline ring targeted to create TAMRA–ANT.

The positioning of ANT's quinoline ring is superimposable with the positioning of the Trp lock's indole ring in PYL–ABA–PP2C complexes, which also engages in π–π/π–cation interactions with homologous residues (Fig. 3 *B* and *C*). These data demonstrate that ANT engages PYL10 with extensive contacts to form a binary complex that positions ANT's quinoline ring in the 4′ tunnel, blocking receptor–PP2C interactions.

Based on prior structural analyses of PYL10 in complex with 3CB, an OP analog that activates all receptor types, we anticipated that ANT's second cyclopropyl substituent might sterically clash with L159, which determines the selectivity of OP for subfamily II/III receptors (21); however, our structure shows that the gate loop adopts a noncanonical closed conformation (*SI Appendix*, Fig. S8*H*) that expands to accommodate ANT's second cyclopropyl and allows

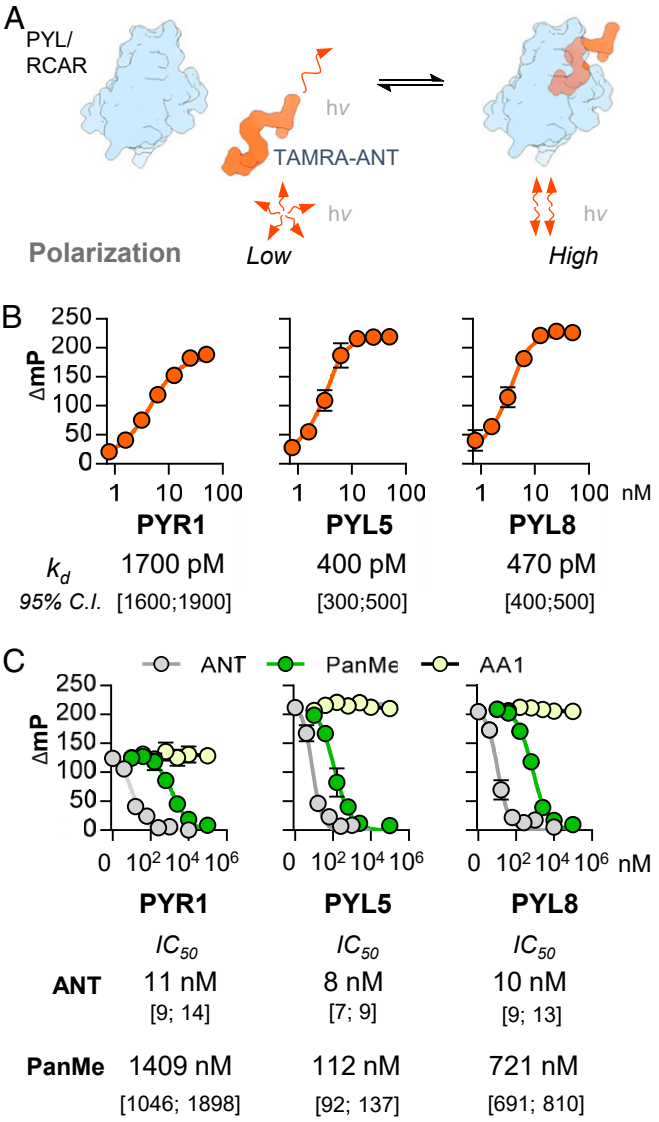

Fig. 4. ANT is a high-affinity ligand. (*A*) Principle of fluorescence polarization-based receptor-binding assays with TAMRA–ANT. Unbound probe polarization is low, due to rapid tumbling in solution; binding of the probe to protein slows tumbling rates and increases fluorescence polarization. (*B*) Determination of equilibrium ABA receptor binding constants for TAMRA–ANT by FP. Delta millipolarization (mP) values for probe (5 nM) as a function of different ABA receptor concentrations (0.8 to 50 nM) in FP assay buffer at 25 °C under equilibrium binding conditions (>4 $t_{1/2}$). We note that the TAMRA–ANT concentrations required for sufficient mP signal generation in these assays are not $<<k_d$; therefore, binding data were fit to the Morrison quadratic equation for single-site ligand binding, rather than the standard Hill equation (see Jarmoskaite et al., ref. 49). Nonlinear fits were conducted in GraphPad Prism, SDs are shown, data are from three independent experiments each conducted with four or more technical replicates. The inferred binding dissociation constants are *Insets* under each graph. (*C*) ANT and PanMe are potent competitors of TAMRA–ANT/receptor interactions. FP competition experiments with 5 nM probe, 10 nM receptor protein, and different competitors, incubated in FP assay buffer at 25 °C for 120 min. Error bars indicate SD ($n = 3$); IC_{50} values are *Insets* under the graphs and inferred by nonlinear fits in drc; 95% confidence intervals are shown below.

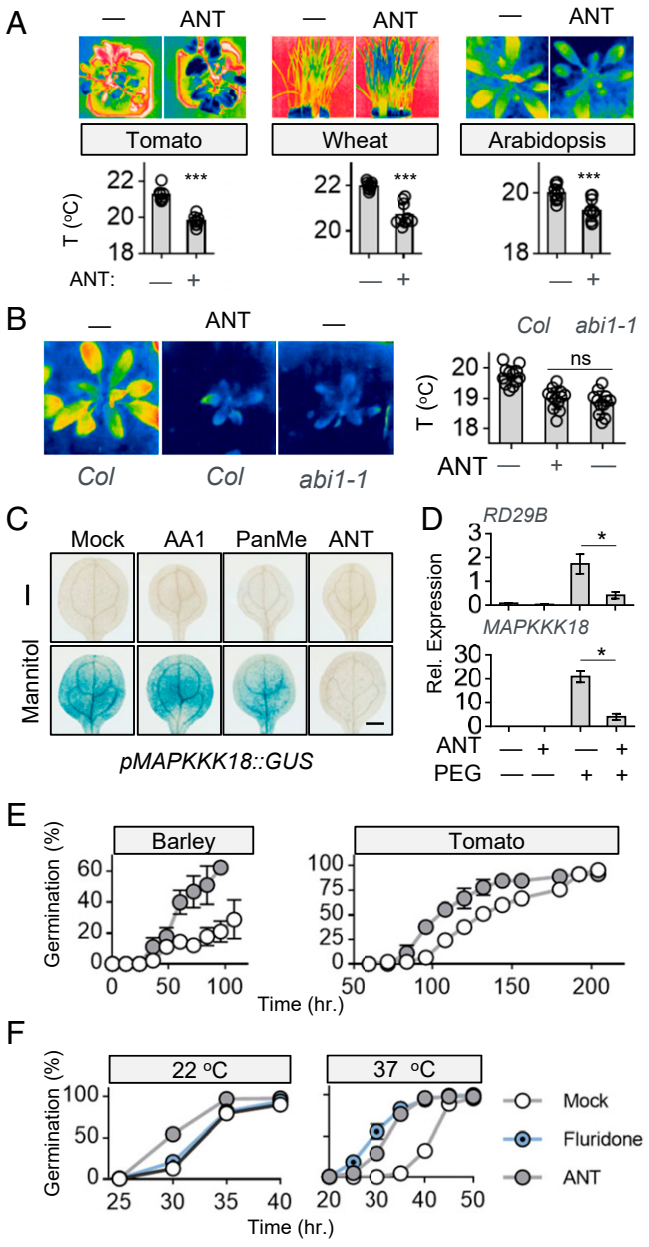

Fig. 5. ANT potently blocks ABA signaling in planta. (*A*) ANT increases transpiration in multiple species. Infrared images of 6-wk-old tomato seedlings (UC82), 3-wk-old wheat seedlings (Patwin 515), and 3-wk-old wild-type *Arabidopsis* (Col-0) plants treated with ANT (100 μM) and imaged by thermography either 2 h (tomato and wheat) or 48 h (*Arabidopsis*) post-application. Statistical analyses were performed using unpaired *t* tests ($n = 8$ for tomato, $n = 9$ for wheat, and $n = 10$ for *Arabidopsis*). Error bars indicate SD. *** indicates $P < 0.0001$. (*B*) ANT treatments phenocopy *abi1-1* mutant phenotypes. Infrared images of wild-type *Arabidopsis* plants continuously exposed to ANT (100 μM) or mock compared to mock-treated *abi1-1*. Images were collected 3 wk after continuous exposure. Dunnett tests were used to obtain multiplicity-adjusted *P* values for treatment effects relative to mock treatments ($n = 12$). (*C* and *D*) ns indicates not statistically significant. ANT blocks osmotic stress–induced gene expression. (*C*) Five-day-old marker line seedlings were treated with 400 mM mannitol for 6 h, with coapplication of either 2.5 μM ANT, PanME, AA1, or mock treatment. (Scale bars, 0.5 mm.) The full dataset for this experiment is presented in *SI Appendix*, Fig. S11. (*D*) Comparison of transcript levels of RD29B and MAPKKK18 (normalized to PEX4) measured by qRT-PCR of 8-d-old *Arabidopsis* seedlings pretreated with either dimethyl sulfoxide (DMSO) or 25 μM ANT for 4 h and then exposed to either DMSO (–) or 25 μM ANT(+) in the presence (+) or absence (–) of 20% PEG for another 6 h. * indicates $P < 0.05$ for indicated comparisons. (*E*) ANT accelerates seed germination. Seed germination was monitored for seeds plated on 1/2 Murashige & Skoog (MS), 0.7% agar plates containing DMSO (mock treated) or 100 μM ANT (barley) or 25 μM ANT (tomato). Time-response data were fit to a log-logistic model using the drc package to infer ET_{50} values; however, barley under mock treatment never reached 50% germination. ET_{50} significantly differs between ANT and mock tomato treatments (two-sample *t* test, $P < 0.01$, $n = 3$) and the percent germination after 4 d significantly differs between ANT and mock-treated Palmella landrace (two-sample *t* test, $P = 0.001$, $n = 3$ for ANT, $n = 6$ for mock). Data for both landraces tested (Morex and Palmella) are shown in *SI Appendix*, Fig. S13. (*F*) ANT alleviates the effects of thermoinhibition in *Arabidopsis*. The ET_{50} values inferred from this experiment are shown in *SI Appendix*, Fig. S13 and were generated by quantifying germination over time for seeds plated on 1/2 MS, 0.7% agar plates containing DMSO (mock treated) or 30 μM test chemicals either at 22 °C or after exposure to heat stress (37 °C for 48 h). Error bars indicate the SEM. Under heat stress, ANT and fluridone ET_{50} values differ from mock (pairwise two-sample *t* test with Bonferroni correction, $P < 0.001$, $n = 5$ for ANT and fluridone, $n = 4$ for mock), and under control conditions ANT ET_{50} significantly differs from fluridone and mock treatments (pairwise two-sample *t* test with Bonferroni correction, $P < 0.001$, $n = 5$ for ANT and fluridone, $n = 4$ for mock).

it to extend into the 3′ tunnel (Fig. 3*C* and *SI Appendix*, Fig. S8*H*), forming hydrophobic contacts with L159. Thus, ANT's reduced selectivity relative to its parent OP is apparently due to subtle changes in gate conformation that ANT, but not OP, stabilizes.

ANT Is a High-Affinity Ligand. Our biochemical assays show that ANT is a particularly strong antagonist that can antagonize micromolar ABA concentrations with EC_{50} values in the mid-nanomolar range (Fig. 2*C*). This implies that ANT–receptor interactions are substantially stronger than receptor/ABA/PP2C interactions, which have been measured in the low-nanomolar range by isothermal titration calorimetry (ITC) (3, 37–39). Determining binding constants for high-affinity ligands can be technically challenging; we, therefore, sought to create a fluorescently tagged ANT derivative for use in fluorescence polarization (FP)–based measurements (40), which measure receptor–ligand complex formation by increased polarization of bound versus free fluorophore (Fig. 4*A*). Exploiting our crystallographic data, we designed a probe with a fluorescent TAMRA label linked to the solvent-exposed C7 site on ANT's quinoline ring (Fig. 3*C*) and used click chemistry to append a TAMRA-5-azide, creating a C7-triazole-ANT analog called TAMRA–ANT (see *SI Appendix*, Fig. S1*C* for synthetic details). To confirm that the attachment of the TAMRA label did not substantially reduce antagonist activity, we tested TAMRA–ANT in PP2C recovery assays and observed near equipotency to ANT against multiple receptor subtypes (*SI Appendix*, Fig. S9*A*). Thus, TAMRA–ANT is a fluorescent ANT derivative that retains tight receptor binding and antagonist activity.

With TAMRA–ANT in hand, we next defined suitable conditions for measuring equilibrium binding constants and conducted titration experiments in the intermediate-binding regime with fixed TAMRA–ANT (5 nM) and varying receptor concentrations (Fig. 4*B* and *SI Appendix*, Fig. S9*B*). Nonlinear fits of these data to the Morrison quadratic binding equation reveal that TAMRA–ANT possesses mid-picomolar to low-nanomolar k_d values for ABA receptors selected from the three angiosperm subfamilies (PYR1 k_d = 1,700 pM; PYL5 k_d = 400 pM; PYL8 k_d = 470 pM; Fig. 4*B*). We further used TAMRA–ANT in competitive displacement assays and observed that ANT displaces TAMRA–ANT from ABA receptors with low nanomolar IC_{50} values and show that it is ∼10 to 100-fold more potent than PanMe under these assay conditions (Fig. 4*C*), comparable to what we observe in PP2C recovery assays (Fig. 2*B*). We note that AA1 does not displace TAMRA–ANT binding, providing further evidence that it is not a high-affinity ABA receptor binder. We independently confirmed this by ITC measurements with AA1 and PYL5, which revealed

negligible enthalpy changes in titrations (*SI Appendix*, Fig. S10); thus, AA1's mechanism of action is unlikely to involve direct ABA receptor binding. Collectively, these data indicate that the ANT scaffold provides unusually high-affinity ABA–receptor binding activity and show that TAMRA–ANT provides a convenient reagent for measuring ligand–receptor interactions by fluorescence polarization. We also note that TAMRA–ANT enables facile and direct titration of active receptor concentrations, which is technically quite valuable since recombinant receptor preparations often contain a significant fraction of inactive receptors, and precise active concentrations are required to calculate accurate k_ds and obtain reproducible IC_{50}s (*SI Appendix*, *Supplementary Materials and Methods* and Fig. S9*C*).

ANT Blocks ABA Signaling In Vivo. Encouraged by the promising activity of ANT in reversing the effects of exogenous ABA in seedling establishment assays (Fig. 1*E* and *SI Appendix*, Fig. S6 *A* and *B*), we investigated the effects of ANT in *Arabidopsis*, wheat, and tomato using quantitative thermal imaging. ANT treatments elicited a decrease in leaf temperature in all three species after a single chemical application (Fig. 5*A*), suggestive of increased transpiration and probable antagonism of guard cell ABA receptors. In addition, continuous ANT treatments mimic the reduced stature and increased leaf temperature phenotypes of the ABA insensitive mutant *abi1-1* (Fig. 5*B*). We next compared the antagonistic effects of ANT, PanMe, and AA1 in vegetative tissues using a reporter line in which β-glucuronidase (GUS) is driven by the promoter of the ABA-responsive gene *MAPKKK18* (*Mitogen-Activated Protein Kinase Kinase Kinase 18*) (24). Using this reporter line, we observed that ANT cotreatments block both exogenous ABA-induced expression and osmotic stress–induced expression of the *pMAPKKK18::GUS* reporter gene and were more active in blocking ABA responses than PanMe or AA1 at the concentration tested (Fig. 5*C* and *SI Appendix*, Fig. S11). Consistent with this conclusion, we observe that ANT pretreatments antagonize osmotic stress (20% polyetheylene glycol-8000 [PEG-8000]) induced gene expression of *MAPKKK18* and *RD29B* transcript levels (Fig. 5*D*). We also examined ANT's effects on ABA-mediated gene expression in wheat seedlings and observe that ANT coapplication with ABA reduces expression of the ABA-responsive genes *TaLea* and *TaPP2C6* (*SI Appendix*, Fig. S12). Collectively, these data show that ANT antagonizes ABA effects in vivo in *Arabidopsis*, wheat, and tomato.

Next, we investigated whether ANT could act as a germination stimulant and measured ANT's effects on seed germination in barley and tomato in the absence of stratification (a dormancy-breaking treatment). These experiments show that ANT treatment lowers the ET_{50} (time to 50% germination) in both species, although in barley the results depended on landrace, suggesting potential genetic variation in seed ABA sensitivity (Fig. 5*E* and *SI Appendix*, Fig. S13). We also examined ANT treatments in *Arabidopsis* to determine whether ANT would similarly accelerate seed germination or prevent the ABA-mediated disruption of seed germination induced by heat stress (thermoinhibition) (41). These experiments included control treatments with fluridone, a carotenoid biosynthetic inhibitor that acts early in the pathway (phytoene desaturation) (42) and disrupts de novo stress-induced ABA biosynthesis (41, 43). Under control germination conditions using nondormant (after ripened) *Arabidopsis* seeds, ANT treatments (but not fluridone treatments) accelerated germination by about 10% (ET_{50} mock = 33 h, ET_{50} ANT = 30 h; $P < 0.001$), suggesting that preexisting ABA pools restrict germination in nondormant *Arabidopsis* seeds, in addition to the well-known role of newly synthesized ABA in restricting germination in imbibed, dormant seeds (44). In seeds exposed to heat stress (37 °C), both ANT and fluridone treatments accelerated seed germination by 9 and 12 h, respectively (Fig. 5*F* and *SI Appendix*, Fig. S13), consistent with the known role of stress-induced ABA in thermoinhibition. Thus, disruption of ABA signaling by ANT disrupts both basal and stress-induced ABA effects, resulting in accelerated seed germination. Collectively, our data show that ANT is effective at disabling ABA signaling in vivo, and that it may be useful in combination with biosynthetic inhibitors to discriminate processes that require de novo biosynthesis from those that do not.

Synthetic modulators of ABA receptors are being actively explored as probes for not only studying ABA dependence in a variety of plant physiological processes but also useful tools in agriculture. We used click chemistry to modify and build upon the scaffold of a potent ABA agonist, OP, to identify a peptidotriazole motif that was subsequently optimized to create, ANT, a pan-ABA receptor antagonist with high bioactivity and receptor binding affinity. Our ANT:PYL10 structure reveals that ANT sterically blocks access to the 4′ tunnel, an important site of binding of a conserved tryptophan from PP2Cs by stabilizing the receptor with multiple contacts in a noncanonical closed conformation. Furthermore, our development of a triazole-based scaffold broadens the chemical space available for manipulating ABA receptor function. ANT is demonstrably more potent and bioactive than PanMe and AA1 in antagonizing multiple ABA-mediated responses in *Arabidopsis* and exhibits bioactivity in multiple crop species such as wheat, barley, and tomato. In particular, ANT's effects as a germination enhancer in barley and tomato may be beneficial agriculturally; however, further toxicological characterization would be required before ANT (or any other antagonist) is suited for agricultural purposes. The pan-antagonistic profile of ANT, though useful in disabling ABA signaling in vivo, limits its use as a tool for dissecting the individual roles of different subfamilies of ABA receptors; the development of selective antagonists for different subfamilies may aid in this endeavor. Nevertheless, ANT is an unusually potent chemical probe for blocking ABA signaling in planta and may have potential applications in research and agriculture. Our development of TAMRA–ANT will also facilitate future biophysical studies of ligand–receptor interactions.

Data Availability. The atomic coordinates and structure factors reported in this article have been deposited in the Protein Data Bank, https://www.wwpdb.org/ [PDB ID codes 7MLC (45) and 7MLD (46)].

ACKNOWLEDGMENTS. Funding for this work was provided by NSF (1656890) (to S.R.C.), US–Israel Binational Agricultural R&D Fund (IS491916R) (to S.R.C. and A.M.), Japan Science and Technology Agency Science and Technology Research Partnership for Sustainable Development (JPMJSA1805), Japanese Society for the Promotion of Science Grants-in-Aid for Scientific Research (17H05009), and the Joint Research Program of Arid Land Research Center, Tottori University (30C2007) (to M.O.).

1. S. R. Cutler, P. L. Rodriguez, R. R. Finkelstein, S. R. Abrams, Abscisic acid: Emergence of a core signaling network. *Annu. Rev. Plant Biol.* **61**, 651–679 (2010).
2. S.-Y. Park *et al.*, Abscisic acid inhibits type 2C protein phosphatases via the PYR/PYL family of START proteins. *Science* **324**, 1068–1071 (2009).
3. Y. Ma *et al.*, Regulators of PP2C phosphatase activity function as abscisic acid sensors. *Science* **324**, 1064–1068 (2009).
4. T. Umezawa *et al.*, Type 2C protein phosphatases directly regulate abscisic acid-activated protein kinases in Arabidopsis. *Proc. Natl. Acad. Sci. U.S.A.* **106**, 17588–17593 (2009).
5. F.-F. Soon *et al.*, Molecular mimicry regulates ABA signaling by SnRK2 kinases and PP2C phosphatases. *Science* **335**, 85–88 (2012).
6. J. D. M. Helander, A. S. Vaidya, S. R. Cutler, Chemical manipulation of plant water use. *Bioorg. Med. Chem.* **24**, 493–500 (2016).
7. W. Dejonghe, M. Okamoto, S. R. Cutler, Small molecule probes of ABA biosynthesis and signaling. *Plant Cell Physiol.* **59**, 1490–1499 (2018).
8. J. Frackenpohl *et al.*, "Use of substituted isoquinolinones, isoquinolindiones, isoquinolintriones and dihydroisoquinolinones or in each case salts thereof as active agents against abiotic stress in plants." US Patent 9,173,395 (2015). https://patentimages.storage.googleapis.com/85/bf/14/6a7bab7007eff7/US9173395.pdf. Accessed 8 September 2021.
9. S. R. Cutler, S. V. Wendeborn, P. J. Jung, M. D. Lachia, R. Dumeunier, "Compounds that induce aba responses." US Patent 2016/0280651 (2016). https://patentimages.storage.googleapis.com/3c/8e/a5/53ecd16d2042a7/US20160280651A1.pdf. Accessed 8 September 2021.
10. S. R. Cutler, M. Okamoto, "Synthetic compounds for vegetative ABA responses." US Patent 9,345,245 (2016). https://patentimages.storage.googleapis.com/0d/77/e5/b485cd4b65b762/US9345245.pdf. Accessed 8 September 2021.

11. M. D. Lachia *et al*., "2-oxo-3,4-dihydroquinoline compounds as plant growth regulators." US Patent 2018/0044297 (2018). https://patentimages.storage.googleapis.com/02/4b/ee/fc4a6a0f677484/US20180044297A1.pdf. Accessed 8 September 2021.
12. J. Frackenpohl *et al*., "Use of substitute oxo tetrahydroquinoline sulfonamides or salts thereof for raising stress tolerance of plants." US Patent 2017/0027172 (2017). https://patentimages.storage.googleapis.com/0d/e0/59/3fb3cd32900682/US20170027172A1.pdf. Accessed 8 September 2021.
13. J. Frackenpohl *et al*., "Use of substituted dihydrooxindolylsulfonamides, or the salts thereof, for increasing the stress tolerance of plants." US Patent 2016/0237035 (2016). https://patentimages.storage.googleapis.com/cb/6e/25/842328f2b2cbef/US20160237035A1.pdf. Accessed 8 September 2021.
14. J. Frackenpohl *et al*., "Substituted 1-cycloalkyl-2-oxotetrahydroquinolin-6-ylsulfonamides or salts thereof and use thereof to increase stress tolerance in plants." US Patent 2018/0020662 (2018). https://patentimages.storage.googleapis.com/6d/43/e5/67dd0ad006b0f2/US20180020662A1.pdf. Accessed 8 September 2021.
15. J. Frackenpohl, L. Willms, J. Dittgen, "Substituted cyano cycloalkyl penta-2, 4-dienes, cyano cycloalkyl pent-2-en-4-ynes, cyano heterocyclyl penta-2, 4-dienes and cyano heterocyclyl pent-2-en-4-ynes as. . .." US Patent Appl. 20170210701A1 (2017). https://patents.google.com/patent/US20170210701A1/en. Accessed 8 September 2021.
16. J. Frackenpohl *et al*., "Aryl-and hetarylsulfonamides as active ingredients against abiotic plant stress." US Patent 2011/0230350 (2011). https://patentimages.storage.googleapis.com/a7/2d/ea/8a60a636e4fdd7/US20110230350A1.pdf. Accessed 8 September 2021.
17. S. R. Cutler, M. D. Lachia, S. V. Wendeborn, C. R. A. Godfrey, D. Sabbadin, "Carbamate quinabactin." World Patent 2018/017490 (2018). https://patentimages.storage.googleapis.com/65/27/d8/68509d60cc0199/WO2018017490A1.pdf. Accessed 8 September 2021.
18. C. R. A. Godfrey, M. D. Lachia, S. V. Wendeborn, D. Sabbadin, "Plant growth regulator compounds." World Patent 2018/007217 (2018). https://patentimages.storage.googleapis.com/87/fd/61/816a6c284d84f1/WO2018007217A1.pdf. Accessed 8 September 2021.
19. S. R. Cutler, S. V. Wendeborn, O. Loiseleur, M. D. Lachia, D. Sabbadin, "Derivatives of halo quinabactin." US Patent 2018/0312470 (2018). https://patentimages.storage.googleapis.com/af/59/c9/c06faa2b1d5db6/US20180312470A1.pdf. Accessed 8 September 2021.
20. A. S. Vaidya *et al*., A rationally designed agonist defines subfamily IIIA abscisic acid receptors as critical targets for manipulating transpiration. *ACS Chem. Biol.* **12**, 2842–2848 (2017).
21. A. S. Vaidya *et al*., Dynamic control of plant water use using designed ABA receptor agonists. *Science* **366**, eaaw8848 (2019).
22. M.-J. Cao *et al*., Combining chemical and genetic approaches to increase drought resistance in plants. *Nat. Commun.* **8**, 1183 (2017).
23. D. Elzinga *et al*., Defining and exploiting hypersensitivity hotspots to facilitate abscisic acid agonist optimization. *ACS Chem. Biol.* **14**, 332–336 (2019).
24. M. Okamoto *et al*., Activation of dimeric ABA receptors elicits guard cell closure, ABA-regulated gene expression, and drought tolerance. *Proc. Natl. Acad. Sci. U.S.A.* **110**, 12132–12137 (2013).
25. J. Takeuchi *et al*., Designed abscisic acid analogs as antagonists of PYL-PP2C receptor interactions. *Nat. Chem. Biol.* **10**, 477–482 (2014).
26. J. Takeuchi *et al*., Structure-based chemical design of abscisic acid antagonists that block PYL-PP2C receptor interactions. *ACS Chem. Biol.* **13**, 1313–1321 (2018).
27. J. Takeuchi, T. Ohnishi, M. Okamoto, Y. Todoroki, Conformationally restricted 3′-modified ABA analogs for controlling ABA receptors. *Org. Biomol. Chem.* **13**, 4278–4288 (2015).
28. J. Takeuchi, H. Nagamiya, S. Moroi, T. Ohnishi, Y. Todoroki, Design of potent ABA receptor antagonists based on a conformational restriction approach. *Org. Biomol. Chem.* **18**, 4988–4996 (2020).
29. Y. Mikame *et al*., Synthesis of all stereoisomers of RK460 and evaluation of their activity and selectivity as abscisic acid receptor antagonists. *Chemistry* **25**, 3496–3500 (2019).
30. C. Che *et al*., APAn, a class of ABA receptor agonism/antagonism switching probes. *J. Agric. Food Chem.* **68**, 8524–8534 (2020).
31. K. Yoshida *et al*., Abscisic acid derivatives with different alkyl chain lengths activate distinct abscisic acid receptor subfamilies. *ACS Chem. Biol.* **14**, 1964–1971 (2019).
32. D. Song *et al*., Development of ABA antagonists to overcome ABA- and low temperature-induced inhibition of seed germination in canola, lentil, and soybean. *J. Plant Growth Regul.* **39**, 1403–1413 (2020).
33. N. Diddi *et al*., 3′-(Phenyl alkynyl) analogs of abscisic acid: Synthesis and biological activity of potent ABA antagonists. *Org. Biomol. Chem.* **19**, 2978–2985 (2021).
34. J. M. Nyangulu *et al*., Synthesis and biological activity of tetralone abscisic acid analogues. *Org. Biomol. Chem.* **4**, 1400–1412 (2006).
35. N. Rajagopalan *et al*., Abscisic acid analogues that act as universal or selective antagonists of phytohormone receptors. *Biochemistry* **55**, 5155–5164 (2016).
36. Y. Ye *et al*., A novel chemical inhibitor of ABA signaling targets all ABA receptors. *Plant Physiol.* **173**, 2356–2369 (2017).
37. J. Santiago *et al*., Modulation of drought resistance by the abscisic acid receptor PYL5 through inhibition of clade A PP2Cs. *Plant J.* **60**, 575–588 (2009).
38. F. Dupeux *et al*., A thermodynamic switch modulates abscisic acid receptor sensitivity. *EMBO J.* **30**, 4171–4184 (2011).
39. I. Szostkiewicz *et al*., Closely related receptor complexes differ in their ABA selectivity and sensitivity. *Plant J.* **61**, 25–35 (2010).
40. M. D. Hall *et al*., Fluorescence polarization assays in high-throughput screening and drug discovery: A review. *Methods Appl. Fluoresc.* **4**, 022001 (2016).
41. S. Toh *et al*., High temperature-induced abscisic acid biosynthesis and its role in the inhibition of gibberellin action in Arabidopsis seeds. *Plant Physiol.* **146**, 1368–1385 (2008).
42. G. Sandmann, A. Schmidt, H. Linden, P. Böger, Phytoene desaturase, the essential target for bleaching herbicides. *Weed Sci.* **39**, 474–479 (1991).
43. T. Gonai *et al*., Abscisic acid in the thermoinhibition of lettuce seed germination and enhancement of its catabolism by gibberellin. *J. Exp. Bot.* **55**, 111–118 (2004).
44. P. Grappin, D. Bouinot, B. Sotta, E. Miginiac, M. Jullien, Control of seed dormancy in *Nicotiana plumbaginifolia*: Post-imbibition abscisic acid synthesis imposes dormancy maintenance. *Planta* **210**, 279–285 (2000).
45. F. C. Peterson, A. S. Vaidya, B. F. Volkman, S. R. Cutler, PYL10 bound to the ABA pan-antagonist 4a. *Protein Data Bank*. https://www.rcsb.org/structure/7MLC. Deposited 28 April 2021.
46. F. C. Peterson, A. S. Vaidya, B. F. Volkman, S. R. Cutler, PYL10 bound to the ABA pan-antagonist antabactin. *Protein Data Bank*. https://www.rcsb.org/structure/7MLD. Deposited 28 April 2021.
47. C. Ritz, F. Baty, J. C. Streibig, D. Gerhard, Dose-response analysis using R. *PLoS One* **10**, e0146021 (2015).
48. S. Salentin, S. Schreiber, V. J. Haupt, M. F. Adasme, M. Schroeder, PLIP: Fully automated protein-ligand interaction profiler. *Nucleic Acids Res.* **43** (W1), W443–W447 (2015).
49. I. Jarmoskaite, I. AlSadhan, P. P. Vaidyanathan, D. Herschlag, How to measure and evaluate binding affinities. *eLife* **9**, e57264 (2020).